Proceedings of ASME Turbo Expo 2011
GT2011
June 6-10, 2011, Vancouver, British Columbia, Canada

GT2011-45579

DETERMINATION OF EQUIVALENCE RATIO AND OSCILLATORY HEAT RELEASE DISTRIBUTIONS IN NON-PREMIXED BLUFF BODY-STABILIZED FLAMES USING CHEMILUMINESCENCE IMAGING

Caleb Cross, Eugene Lubarsky, Dmitriy Shcherbik, Keary Bonner, Alex Klusmeyer and Ben T. Zinn
Georgia Institute of Technology
Atlanta, GA, USA

Jeffery A. Lovett
Pratt & Whitney Aircraft Engines
East Hartford, CT, USA

ABSTRACT

In an effort to elucidate the fundamental processes controlling bluff body flame stabilization, the dependence of the spatial distribution of the local equivalence ratio and the heat release dynamics upon the mode of fuel injection was studied. Experiments were performed in a single flame holder combustion channel which was supplied with a high-temperature air stream. Jet-A fuel was injected across the incoming air stream from one of two locations: a cylindrical fuel bar installed 0.25 m upstream of the bluff body, or from fuel injectors integrated within the bluff body 2.5 cm upstream of the trailing edge (i.e., close-coupled injection). The time-averaged spatial distributions of the combustion heat release were characterized by CH* and C_2* chemiluminescence imaging of the flame, and ratios of the C_2* to CH* light emission were used to characterize the local equivalence ratio. The spatial average of the C_2*/CH* value in the flame was found to increase linearly with increasing global equivalence ratio for fuel injection upstream of the bluff body, whereas this value was relatively constant for close-coupled injection. This constant value equaled the same average C_2*/CH* value obtained for upstream fuel injection at globally stoichiometric conditions, suggesting that combustion resulting from close-coupled fuel injection took place, on average, in stoichiometric flamelets throughout the combustor.

The heat release dynamics due to asymmetric (von Kármán) vortex shedding were also investigated for each operating condition by recording high-speed movies of the flame at 24 kHz. Upon processing of these movies, the amplitudes of heat release fluctuations due to von Kármán vortex shedding were found to be significantly higher for close-coupled injection than for injection well upstream of the flame holder for all operating conditions. This is attributed to an increase in span-wise fuel-air mixing and near-wake heat release for upstream fuel injection, resulting in a hotter recirculation zone which suppressed the von Kármán instability more than the close-coupled case.

NOMENCLATURE

a.u.	=	arbitrary units
BVK	=	Bénard/von-Kármán
f	=	frequency
Q' / Q_{mean}	=	oscillatory heat release amplitude normalized by mean heat release
St	=	Strouhal number = $\dfrac{f \cdot W}{V_{in}}$
T_b/T_u	=	ratio of burned to unburned temperatures
T_{in}	=	inlet temperature of air supply
V_{in}	=	inlet velocity
W	=	bluff body width
x	=	distance downstream of bluff body trailing edge
ρ_u/ρ_b	=	ratio of unburned to burned gas densities
Φ_{global}	=	global equivalence ratio in test section
Φ_{local}	=	local equivalence ratio in the flame

INTRODUCTION

Bluff body-stabilized flames are commonly used in propulsion, power generation and a wide range of industrial and domestic energy conversion systems to produce stable, efficient and low pressure loss combustion over wide ranges of operating conditions (e.g., pressures and inlet velocities) and system scales. Because of its common use, extensive research has been performed on bluff body-stabilized flames [1-5]. Most of the understanding of the fundamental processes controlling bluff body flame stabilization has been established for combustion of premixed reactant streams, yet many practical combustion systems utilize non-premixed reactants, such as liquid-fuelled combustors in aircraft engines. In fact, the inlet temperatures in many gas turbine systems have become so high that premixing the fuel is no longer viable because of autoignition concerns. Thus, there is a need to obtain improved understanding of the fundamental processes controlling combustion process stabilization in non-premixed bluff body-stabilized flames. Such understanding may suggest approaches for increasing the ranges of stable operating conditions for practical combustion systems, as well as methods for reducing the amount of harmful emissions, such as NOx.

In particular, knowledge of the spatial and temporal heat release and fuel-air ratio distributions in such systems is needed, as spatial and temporal non-uniformities of these two parameters are likely when the fuel is not uniformly mixed with the oxidizer prior to burning. However, both are difficult (if not impossible) to measure directly. In practice, heat release is usually characterized indirectly by measuring some quantity that is proportional to the amount of fuel burned [6]. One of the most commonly used diagnostic techniques for characterizing heat release in hydrocarbon flames is measuring flame chemiluminescence, which is the spontaneous light emission from electronically-exited radicals which exist in the reaction zone. Radiation from such species typically has wavelengths in the ultraviolet and visible spectra. In hydrocarbon flames, OH*, CH* and C_2* are typically used to gain information about the state of the reaction, since the characteristic lifetimes of these radicals are very short relative to typical residence times in combustors [7]. CH* and OH*, in particular, have been extensively used as qualitative measures of heat release, as previous studies have shown the amount of light emitted from these radicals to be proportional to the amount of fuel consumed, though there is some equivalence ratio dependence [6-8].

Ratios of light emission from various chemiluminescence species have been shown to be proportional to the fuel-air ratio in hydrocarbon flames. Early studies by Clark showed the integrated C_2*/CH* ratio to increase with increasing equivalence ratio for propane-air and ethylene-air flames [9]. Since then, both CH*/OH* and C_2*/CH* have been shown to be reasonably good indicators of equivalence ratio in premixed [10-11] and liquid-fuelled flames [7]. Interestingly, Roby et al. demonstrated these ratios to be linear functions of the overall equivalence ratio for premixed, turbulent flames [11], and Morrell et al. demonstrated the same result for liquid-fuelled, swirl-stabilized flames [7]. However, it should be noted that not all investigators reported linear trends. In fact, Nori and Seitzman show CH*/OH* to be proportional to equivalence ratio in methane-air flames only over a limited range of lean equivalence ratios, and only at certain pressures and temperatures [10].

The goal of this study was to characterize the spatial distributions of heat release and local equivalence ratio in liquid-fuelled bluff body-stabilized flames of various fuel injection configurations. This was done using chemiluminescence imaging of the flame to measure light emission from CH* and C_2* radicals, and ratios of C_2* to CH* were used to characterize the local fuel-air ratio. Two modes of fuel injection were investigated. The first fuel injection configuration involved injecting Jet-A well upstream of the bluff body, giving the fuel sufficient time to evaporate and mix with the high-temperature incoming air stream before reaching the bluff body flame. In the second mode of fuel injection, the Jet-A was injected from four fuel injectors integrated within the bluff body 2.5 cm upstream of the trailing edge. This configuration, referred to as “close-coupled” injection, allowed very little time for the fuel to evaporate and mix before reaching the flame. Images of CH* and C_2*/CH* were compared to identify differences in fuel-air ratio and heat release distributions between the two fuel injection configurations at similar operating conditions.

In addition, this paper will present results from a continuing study of oscillatory heat release due to asymmetric (von Kármán) vortex shedding from the bluff body. In our last paper [12], it was demonstrated that the amplitude of such heat release oscillations increased with increasing global fuel-air ratio for close-coupled fuel injection. This was attributed to a decrease in near-wake heat release with increasing fuel jet penetration into the cross-flow, which resulted in a significant reduction in gas expansion in the shear layers. In this study, we will compare the Bénard/von Kármán (BVK) heat release dynamics between the two fuel injection configurations in order to further elucidate the influence of fuel distribution and subsequent heat release on the vortex shedding process. High-speed photography was used to characterize the oscillatory burning, and processing of these movies using two-dimensional Fourier Transforms allowed for determination of the amplitudes and frequencies of heat release oscillations.

METHODOLOGY

Description of Test Facility, Flame Holder and Fuel Injection Configurations

Experiments were performed in the single flame holder combustion test rig described previously in Ref. 12. A high-temperature, vitiated air stream was supplied to the 7.6 x 15.2 cm rectangular test section by means of a primary burner located 0.7 m upstream of the bluff body. Inlet conditions typically range from a velocity between 100 and 300 m/s, temperature from 700°C to 900°C, and oxygen content between 11 and 16%. All testing is performed at pressures slightly above atmospheric. The test section is ~1.5 m long and has a 0.9 m quartz window section for optical access to the combustion region downstream of the flame holder. The flame holder configuration utilized in this study consisted of an elliptical leading edge and a rectangular trailing edge, shown schematically in Figure 1. The bluff body was 4.75 cm in height and extended the entire span of the test section, providing a blockage ratio of ~ 31%.

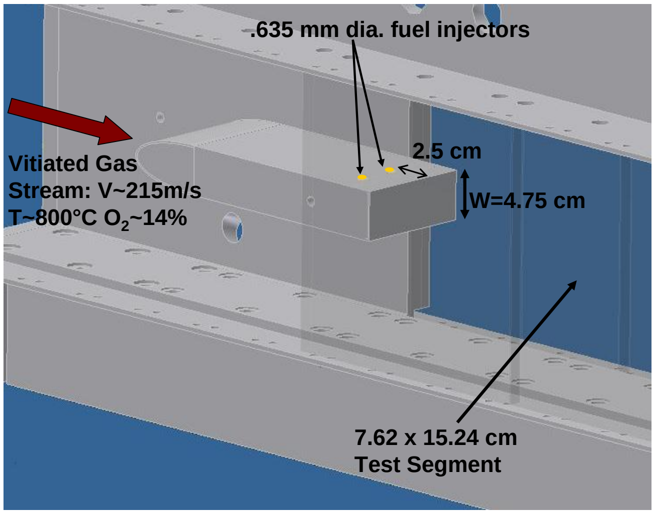

FIGURE 1: SCHEMATIC OF TEST RIG WITH CLOSE-UP VIEW OF FLAME HOLDER, SHOWING KEY DIMENSIONS

Two types of experiments were performed. In the first, liquid Jet-A fuel was injected across the incoming gas stream from a 6.35 mm cylindrical fuel bar located upstream of the bluff body (0.5 m from the trailing edge). The fuel bar had six plain-orifice injectors (3 on each side) which were 0.5 mm in diameter and spaced 19 mm apart from one another. In the second experiment, the fuel was injected by four plain-orifice fuel injectors integrated within the bluff body located 2.5 cm upstream of its trailing edge, as shown in Figure 1. The fuel injectors in this "close-coupled" configuration were .635 mm in diameter, with two injectors located on each side of the bluff body, spaced 2.5 cm apart. A cartoon illustrating these fuel injection configurations is shown in Figure 2. The fuel supply system was set up in a manner which allowed the fuel injection to be immediately altered between locations during testing.

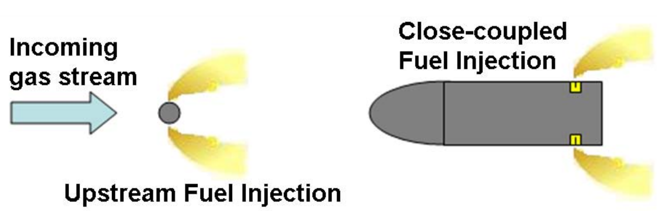

FIGURE 2: SCHEMATIC OF FUEL INJECTION CONFIGURATIONS UTILIZED IN THIS STUDY (NOT DRAWN TO SCALE)

Time-averaged Chemiluminescence Imaging using Three-Camera Spectrometry

Spatial distributions of the time-averaged heat release were characterized using the chemiluminescence imaging system shown schematically in Figure 3. This system contains three cameras (1600 x 1200 pixel spatial resolution) which take wavelength-specific images of the flame, with a field of view covering the entire 0.9 x 0.15 m transparent section of the combustor. Two of the cameras are monochromatic and are equipped with narrow band-pass filters to collect light intensity in wavelengths containing C_2* ($504 < \lambda < 521$ nm) and CH* ($422 < \lambda < 432$ nm) chemiluminescence, respectively. The third camera is a color camera equipped with two triple-band pass filters (see Figure 3 for wavelengths) to collect flame radiation in three specific narrow bands for subtraction of background radiation (due to CO_2* broadband emission and thermal emission) from the CH* and C_2* images [12]. These "pedestal" bands are shown in the Jet-A flame emission spectrum of Figure 4. For each operating condition, 10 images of the flame were recorded by each camera with an exposure time of 10 ms, resulting in a total exposure time of 0.1 s when averaged. An image processing algorithm was developed to average the images, correct for fixed pattern noise and subtract the background radiation from the CH* and C_2* images. The resulting CH* and C_2* images were used to characterize the stationary heat release, and ratios of C_2* to CH* were used as a measure of the local equivalence ratio in the flame. Upon post-processing of the images, "false color" maps are typically applied to the images to facilitate visual comparisons of the heat release and fuel-air ratio distributions.

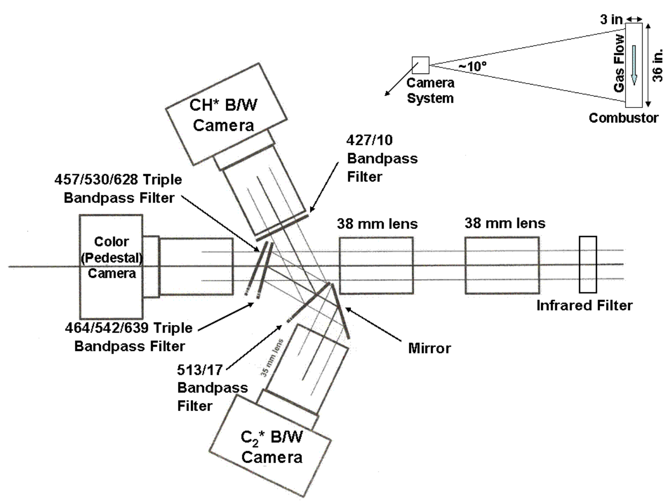

FIGURE 3: SCHEMATIC OF THREE-CAMERA CHEMILUMINESCENCE IMAGING SYSTEM

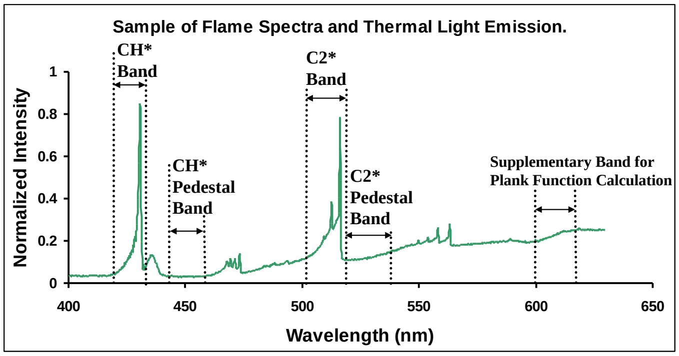

FIGURE 4: MEASURED JET-A FLAME SPECTRUM AND EMISSION BANDS USED FOR IMAGE PROCESSING

Characterization of Heat Release Oscillations Using High-Speed Imaging

High speed movies of the flame were recorded using a NAC GX-1 high-speed camera at a frame rate of 24,000 Hz, a spatial resolution of 400 x 128 pixels and an exposure time of 10μs. These movies were processed using the methodology described previously in Ref. 12. This method produced a time history of the flame luminosity at each axial location in the combustor. This was done by extracting 1 pixel-wide "strips" from each frame in the movie sequence at the given axial location and placing these strips in a new image in chronological order, as illustrated in Figure 5. The red color signal was digitally filtered out of this time history so that only light intensity in blue and green color channels of the camera, which contain CH* and C_2* chemiluminescence, were monitored. The blue and green signals were then averaged to produce a monochromatic flame time history.

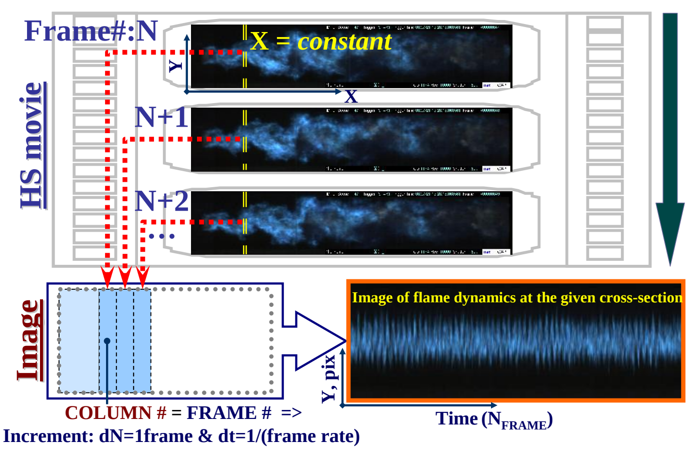

FIGURE 5: METHODOLOGY FOR RECORDING FLAME LUMINOSITY TIME HISTORY AT A GIVEN CROSS-SECTION

A two-dimensional FFT was performed on each time history to obtain the frequencies and amplitudes of the dominant modes of heat release oscillations [12]. Of particular interest in this study was the amplitude of heat release oscillations due to asymmetric (von Kármán) vortex shedding. The maximum amplitude in the resulting 2D FFT at frequencies characteristic of the BVK instability ($0.20 \leq St \leq 0.27$) was used as a measure of the BVK heat release oscillation intensity. This value was normalized by the mean (DC) component of the 2D FFT to eliminate the effects of luminosity, which changed with changing operating conditions (e.g., fuel flow rates). The resulting normalized amplitude is a measure of the oscillatory motion of the flame in the transverse direction, as well as the amount of time these harmonic oscillations persisted throughout the movie sequence.

Experimental Procedure

The spatial and temporal distributions of the combustion process heat release were characterized and compared between the two fuel injection configurations described previously. Two values of the approach velocity to the bluff body test section were tested: 125 and 150 m/s. The temperature of the incoming vitiated gas stream was approximately 800°C for all operating conditions. The global equivalence ratio was varied from 0.30 to 1.20 in increments of approximately 0.15. For each increment of Φ_{global} the fuel supply was switched between upstream and close-coupled fuel injection modes during the test, and the stationary and dynamic heat release were characterized for each fuel injection configuration at each increment of Φ_{global}. Varying the fuel injection location during the test helped reduce the amount of discrepancy in operating conditions between fuel injection modes, allowing for more accurate comparisons of the stationary and dynamic heat release. Such comparisons are given in the next section.

RESULTS AND DISCUSSION

Spatial Distributions of Heat Release and Local Equivalence Ratio

Examples of time-averaged, spatial distributions of CH* and C_2*/CH* chemiluminescence are shown in Figures 6 and 7, respectively. The images compare results obtained for fuel injection upstream of the bluff body (left) to those obtained for close-coupled fuel injection (right) for three values of the global equivalence ratio: 0.31, 0.61 and 0.92. All images shown were taken at an inlet velocity of 125 m/s. These images reveal several key differences in the spatial heat release distributions between the two fuel injection configurations. For example, fuel injection upstream of the bluff body typically resulted in stronger CH* intensities in the shear layers than close-coupled fuelling. For close-coupled fuelling, the peak CH* intensity typically occurred along the centerline of the combustor several bluff body widths downstream.

With the exception of the leanest overall fuel-air ratio, fuel injection upstream of the bluff body resulted in a greater overall CH* intensity than close-coupled injection at identical operating conditions. This is attributed, in part, to an increase in combustion efficiency due to the fuel being vaporized and well-mixed prior to burning for upstream injection, whereas the combustion process was limited by fuel-air mixing for close-coupled fuelling. The low CH* signal that occurred for Φ_{global}=0.31 with upstream fuel injection is due to the lean local equivalence ratio that existed throughout the reaction zone, which resulted in a substantially weaker CH* distribution than its close-coupled counterpart even though the fuel flow rates were nearly identical [8, 10] (it will be shown that the local equivalence ratios for close-coupled injection were typically near stoichiometric, regardless of the global fuel-air ratios).

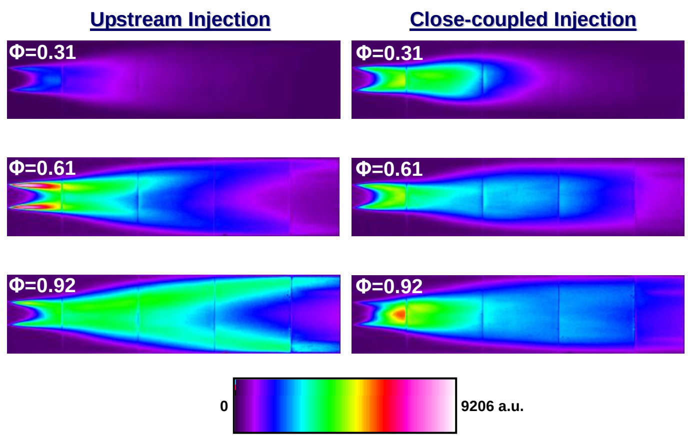

FIGURE 6: CH* IMAGES FOR UPSTREAM (LEFT) AND CLOSE-COUPLED (RIGHT) FUEL INJECTION MODES FOR V_{IN}=125 M/S. GLOBAL EQUIVALENCE RATIOS FOR EACH CASE ARE SHOWN IN THE IMAGES.

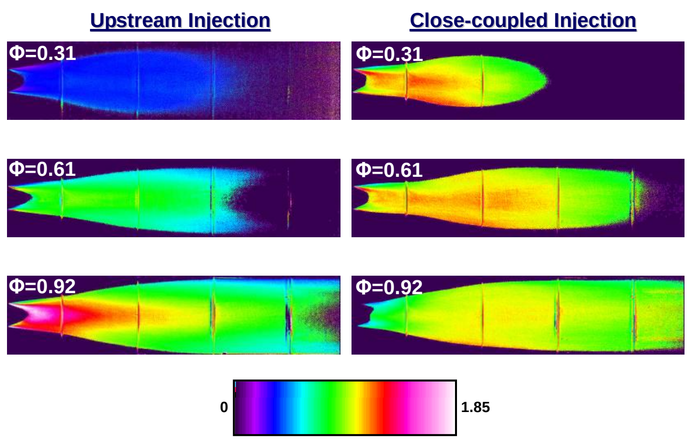

FIGURE 7: C_2*/CH* IMAGES FOR UPSTREAM (LEFT) AND CLOSE-COUPLED (RIGHT) FUEL INJECTION MODES (SAME OPERATING CONDITIONS AS FIGURE 6)

The C_2*/CH* images of Figure 7 suggest significant differences occurred in the local equivalence ratio distributions between the two fuel injection configurations. For fuel injection upstream of the bluff body the C_2*/CH* values increased throughout the flame with increasing Φ_{global}, as is expected when the fuel is well-mixed prior to burning. However, the C_2*/CH* distribution became more and more non-uniform as the global equivalence ratio was increased. This is most evident in the Φ_{global}=0.92 image, where a pocket of high C_2*/CH* ratios is seen to have occurred in the near-wake region, whereas further downstream the mixture appears to have burned at leaner local fuel-air ratios. This high C_2*/CH* value in the near-wake could be an accurate indication of locally rich combustion due to non-uniform fuel-air mixing, or it could possibly be an erroneous measurement due to the existence of secondary diffusion flames within the recirculation zone [11] or the recirculation of rich combustion products, both of which possibly distorting the C_2*/CH* signal. Further work is needed to identify the source(s) of these non-uniformities in C_2*/CH* for fuel injection upstream of the bluff body.

On the other hand, the C_2*/CH* distributions for close-coupled fuel injection were very similar for all values of Φ_{global} (other than the fact that the length of the reaction zone increased with increasing Φ_{global}). The most significant changes in the spatial C_2*/CH* distributions for close-coupled fuel injection occurred in the near-wake region. As Φ_{global} was increased, the C_2*/CH* signal in the near-wake region of the flame decreased, suggesting that the local fuel-air ratio became leaner in this region due to increasing fuel jet penetration into the cross-flow, and as a result, less fuel entrainment into the near-wake [12].

Determination of Average C_2*/CH* Signal in the Flame

In order to provide more quantitative comparisons, the average C_2*/CH* signal in the flame was calculated for each operating condition. The procedure for determining this value was as follows. First, the original CH* and C_2* images were filtered by setting any pixel intensity less than a threshold value to zero. The threshold for each image was chosen to be 10% of its maximum pixel intensity (thus varying between each image due to differences in overall luminosity). Next, the filtered C_2* image was divided by the filtered CH* image for the same operating condition, and the C_2*/CH* values were summed throughout the image (if CH*=0 at a particular point after applying the threshold, C_2*/CH* was set to zero at that location). Finally, this sum was divided by the number of pixels in the filtered image with nonzero C_2*/CH* values. The resulting value was the average C_2*/CH* value in the reaction zone and did not include contributions from locations in which the chemiluminescence signal was low (e.g., the recirculation zone and image corners).

This value was determined for each operating condition (i.e., inlet velocity, overall fuel-air ratio and fuel injection configuration) and is plotted as a function of the global equivalence ratio in Figure 8. Interestingly, the average C_2*/CH* value was found to increase linearly with increasing global equivalence ratio when the fuel was injected upstream of the bluff body. Furthermore, these values did not vary considerably when the incoming velocity was increased to 150 m/s, further supporting its use as an indicator of equivalence ratio. It is worth noting that Morrell et al. also reported a linear increase in integrated C_2*/CH* values with increasing equivalence ratio for a liquid-fuelled (n-heptane) swirl-stabilized flame [7].

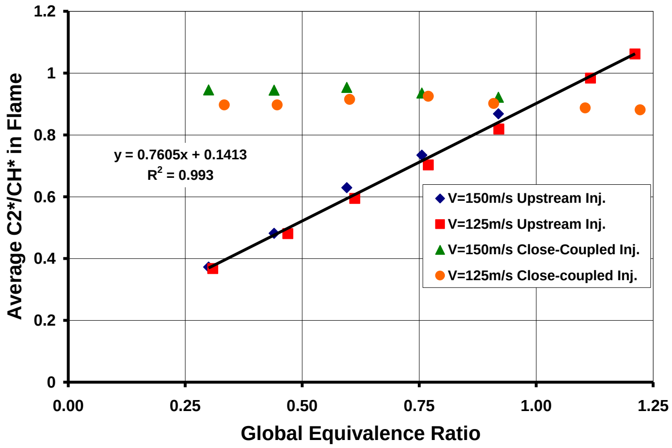

FIGURE 8: AVERAGE C_2*/CH* IN THE FLAME VS. GLOBAL EQUIVALENCE RATIO

The linear dependency of the average C_2*/CH* ratio upon the global fuel-air ratio for upstream fuel injection suggests that the fuel was well mixed with the vitiated air stream prior to reaching the flame, burning in either fully or partially-premixed modes of combustion. It also supports the use of C_2*/CH* as a qualitative measure of equivalence ratio in hydrocarbon flames and even suggests the possibility that C_2*/CH* values can be calibrated to yield quantitative values of Φ_{local} for Jet-A combustion. Additional work is needed to verify the latter statement, and it is believed that such a calibration would be very specific to the situation being investigated. That is, it is believed to depend upon additional factors such as vitiation levels, dilution and/or product recirculation, and the diagnostic system utilized [7, 11]. However, if successful, such a calibration would provide a key tool for researchers and designers of practical combustion systems, as estimates of the local fuel-air ratios could be obtained solely by naturally-occurring flame radiation.

In contrast, the spatial averages of C_2*/CH* for close-coupled fuelling were found to be nearly the same for all operating conditions, regardless of the global equivalence ratio. Figure 8 shows only slight variation in this value with varying Φ_{global}. What is of greater interest, however, is that this approximately constant value equaled the same average C_2*/CH* value obtained when the fuel was injected upstream of the flame holder at globally stoichiometric conditions. This suggests that combustion resulting from close-coupled injection took place, on average, in stoichiometric flamelets throughout the combustor, regardless of the overall equivalence ratio. This result is analogous to classical diffusion flames, in which the reaction occurs at locations in which the local equivalence ratio is unity [13]. However, in this case the reaction is believed to be primarily controlled by turbulent mixing of the evaporated fuel with the vitiated air stream, rather than mass diffusion.

Heat Release Dynamics due to Asymmetric Vortex Shedding

High-speed movies of the flame were recorded for each operating condition and fuel injection configuration in which time-averaged chemiluminescence imaging was performed. This was done in order to determine the dependence of the von Kármán-associated heat release oscillation amplitudes upon the mode of fuel injection and overall equivalence ratio. Figure 9 shows a comparison of frames extracted from high-speed movies for Φ_{global}=0.61 and V_{in}=125 m/s, comparing instantaneous luminosity images resulting from the two different fuel injection modes. These images reveal distinct differences in flame structure. Upstream fuel injection resulted in flame stabilization in two distinct, symmetric shear layers downstream of the bluff body, as seen in the top image of Figure 9. This shear layer flame extends with a very shallow flame angle (practically horizontal) several bluff body widths downstream before minor perturbations are seen. Upon viewing this movie, sinusoidal heat release oscillations presumably due to von Kármán vortex shedding were observed only intermittently, with the majority of frames in the movie showing no clear evidence of coherent, BVK instabilities.

Contrarily, the image extracted from the high-speed movie for the close-coupled case (bottom image of Figure 9) shows clear evidence of heat release fluctuations due to von Kármán vortex shedding. Sinusoidal perturbations are seen to begin 1-2 bluff body widths downstream, and this undulating flame structure is seen to persist throughout the remainder of the camera field of view. These BVK flame oscillations persisted for almost the entire movie sequence.

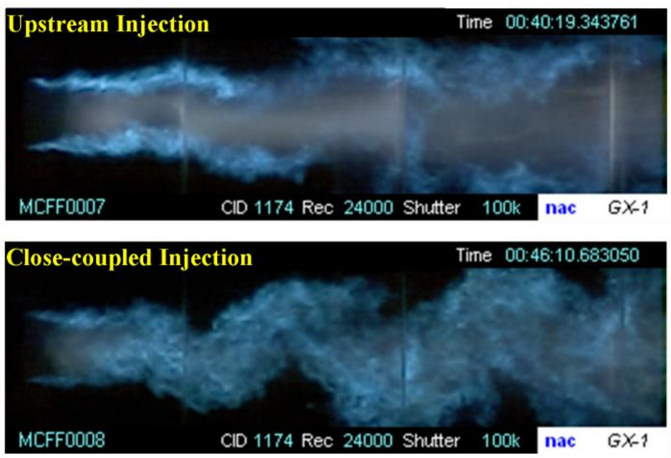

FIGURE 9: COMPARISON OF INSTANTANEOUS FRAMES FROM HIGH-SPEED MOVIES RECORDED FOR UPSTREAM (TOP) AND CLOSE-COUPLED (BOTTOM) FUEL INJECTION AT Φ_{GLOBAL}=0.61 AND V_{IN}=125 M/S

Other key differences can be seen in the general flame structures shown in Figure 9. For example, upstream fuel injection resulted in high intensity flame luminescence in the near-wake shear layers, indicating the presence of large combustion heat release there. This trend was demonstrated previously in the CH* images of Figure 6. However, the light intensity emitted from the near-wake region between the “bright” shear layers (likely due to thermal emission from combustion products) is low, suggesting that little heat release occurs in this region. This image suggests that in this case practically all of the fuel reaching the shear layers is likely consumed there with practically no fuel reaching and burning in the recirculation zone. In contrast, when close-coupled fueling is used, the reaction zone seems to be distributed throughout the flow field. The presence of blue flame luminescence just behind the bluff body indicates that a fraction of the fuel “bypasses” the shear layers and reacts within the recirculation zone.

While images such as those shown in Figure 9 provide qualitative comparisons of flame structure, more quantitative analyses of the amplitudes and frequencies of the BVK-associated heat release oscillations were performed using the previously described high-speed movie processing methodology [12]. Plots of the downstream variation of the BVK heat release oscillation amplitude are shown in Figure 10, comparing upstream and close-coupled fuel injection at Φ_{global}=0.61 and V_{in}=125 m/s (i.e., the same movies shown in Figure 9). From this figure, it can be seen that the spectral amplitude of heat release oscillations due to asymmetric vortex shedding were significantly higher for close-coupled fuel injection than upstream injection at this operating condition. The maximum amplitude for the close-coupled case was ~ 3.75% of the mean luminosity and occurred at 178 mm downstream. Contrarily, upstream injection had maximum amplitude of 1.25% of the mean brightness and had its peak around 127 mm.

Flame luminosity power spectra taken at these axial locations further reflect the differences in BVK heat release oscillation amplitudes between fuel injection modes, see Figure 11. Upstream injection at Φ_{global}=0.61 and V_{in}=125 m/s resulted in a coherent spike in the resulting power spectrum at ~ 1000 Hz, but its amplitude was relatively small, being slightly above 1% of the mean luminosity. However, close-coupled injection at the same operating conditions resulted in a well-pronounced peak at the BVK frequency much higher in magnitude than the background luminosity. These differences in flame response demonstrate the strong dependence of the BVK heat release oscillation amplitude upon the mode of fuel injection.

The maxima of the heat release oscillation amplitudes from plots similar to those shown in Figure 10 were used in this study as a measure of the overall intensity of BVK heat release oscillations for each operating condition. Figure 12 contains a plot of these maxima versus global equivalence ratio (along with best-fit trend lines) for each fuel injection configuration. This graph shows that heat release oscillations due to BVK vortex shedding were significantly higher for close-coupled fuel injection than for upstream injection for all but the leanest global equivalence ratio tested. Figure 12 shows that the intensity of BVK-associated heat release oscillations generally increased with increasing global equivalence ratio for close-coupled fuel injection, reaching a maximum just before blow out of the combustion process, which occurred at Φ_{global} ~ 1.25.

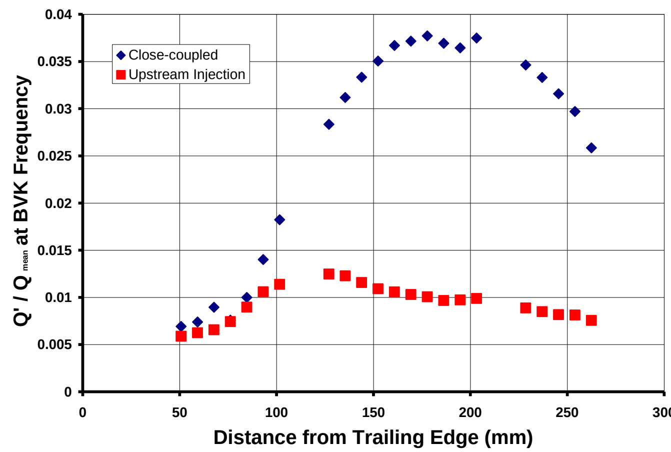

FIGURE 10: AXIAL DISTRIBUTIONS OF THE BVK HEAT RELEASE OSCILLATION AMPLITUDE FOR Φ_{GLOBAL}=0.61 & V_{IN}=125 M/S COMPARING FUEL INJECTION MODES

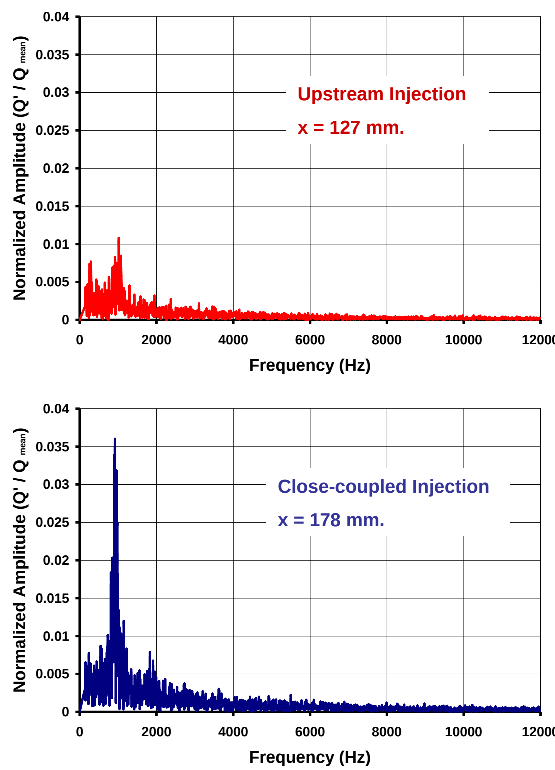

FIGURE 11: COMPARISON OF FLAME LUMINOSITY SPECTRA EXTRACTED FROM HIGH-SPEED MOVIE FFT'S FOR UPSTREAM (TOP) AND CLOSE-COUPLED (BOTTOM) FUEL INJECTION (SAME FLOW CONDITIONS AS FIG. 10)

At this condition, the spectral amplitude at the BVK frequency was very high, exceeding 7% of the mean luminosity. The dynamics resulting from upstream fuel injection exhibited different trends, with the highest heat release oscillation intensities occurring for overall lean and rich operation, but these intensities were minimal in the middle of the operating window ($0.6 < \Phi_{global} < 0.8$). Some possible reasons for these trends are discussed in the next sections. For now, it is worth pointing out that BVK heat release oscillations were strong (~4.5% of mean luminosity) near lean blow out for upstream fuel injection. This is in agreement with previous studies of premixed bluff body-stabilized flames, which demonstrated vortex shedding to occur near blow out [14-16].

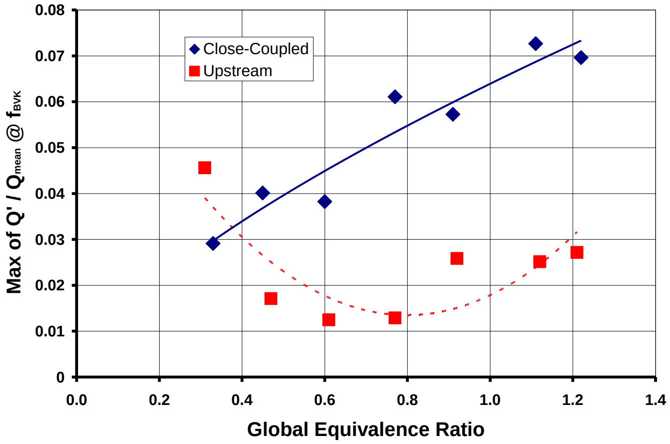

FIGURE 12: MAXIMA OF BVK HEAT RELEASE OSCILLATION AMPLITUDES VERSUS GLOBAL EQUIVALENCE RATIO FOR V_{IN}=125 M/S, COMPARING FUEL INJECTION MODES

Comparison of Spatial and Temporal Heat Release Distributions

In our last paper [12], it was shown that operating conditions resulting in high-amplitude heat release oscillations due to asymmetric vortex shedding also had low CH* intensity occurring in the near-wake shear layers (based on analysis of time-averaged chemiluminescence images). Conversely, when the time-averaged CH* intensity in the shear layers was high, the amplitude of the von Kármán heat release oscillations were low. These results suggest that the amplitudes of BVK-associated heat release oscillations are governed by the amount of heat release occurring in the near-wake region of the flame, with high amounts of heat release due to combustion suppressing the instability by means of gas expansion (dilatation) across the flame [12, 17-18].

A similar analysis was performed in this study in an effort to explain the significant differences in heat release dynamics between the two fuel injection configurations. The amount of heat release occurring in the near-wake shear layers was evaluated by integrating the time-averaged CH* intensities occurring in the two rectangular areas shown in Figure 13a. Each rectangle was 2 by 0.5 bluff body widths in area. The left edges of the rectangles were aligned with the trailing edge and were centered vertically at each corner of the bluff body. It can be seen from the figure that these two rectangular “boxes” encompass the near-wake shear layer regions of the flame.

Figure 13b shows a comparison of the BVK heat release oscillation intensities (from Fig. 12) with the corresponding time-averaged CH* intensities occurring in the near-wake shear layers for each operating condition. From this graph, a general trend can be seen in that the BVK heat release oscillation amplitude decreased with increasing near-wake CH* intensity, providing further evidence of the damping nature of near-wake heat release on the BVK flame dynamics.

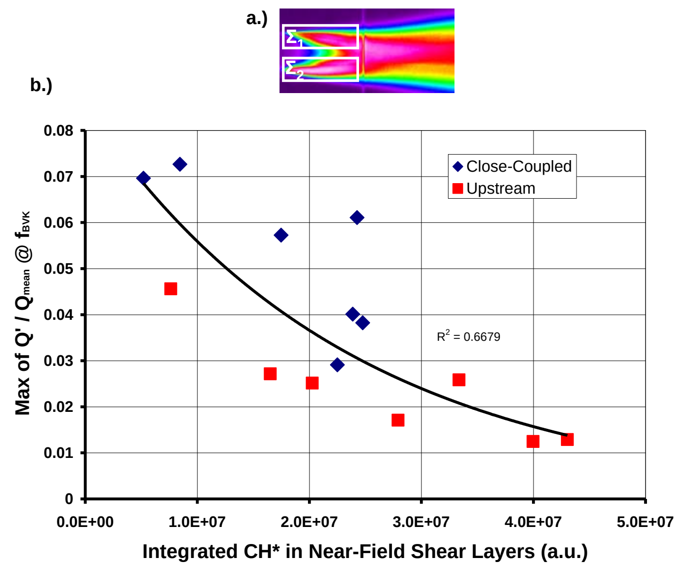

FIGURE 13: a.) OUTLINE OF AREA CHOSEN FOR NEAR-WAKE SHEAR LAYER CH* INTEGRATION
b.) COMPARISON OF MAXIMUM BVK HEAT RELEASE OSCILLATION AMPLITUDE WITH INTEGRATED NEAR-WAKE SHEAR LAYER CH* INTENSITY

Hypothesized Processes Controlling Spatial and Temporal Heat Release Distributions

Figures 12 and 13 show that, in general, upstream fuel injection resulted in significantly lower amplitude BVK heat release oscillations and increased near-wake CH* intensity when compared to close-coupled fuelling. This is attributed to differences in spatial distributions of fuel and consequent heat release between the two fuel injection configurations. Injecting the fuel well upstream (~10 bluff body widths) of the flame holder allowed more time for the fuel to evaporate and mix with the incoming preheated gas stream prior to burning. This increased mixing distance also allowed for the fuel to spread more evenly across the span of the combustor before reaching the reaction zone behind the bluff body, and the resulting flame is postulated to have extended the span of the combustor, as illustrated in the cartoon of Figure 14b. Contrarily, close-coupled fuel injection allowed for very little time for the fuel to mix with the gas stream before burning, due to the proximity of the injection point to the reaction zone. The use of only two injectors on each side of the flame holder likely resulted in non-uniform fuel distribution across the combustor span in the near-wake. Consequently, it is believed that this resulted in two distinct flame sheets emanating from the trailing edge of the bluff body, as illustrated in Figure 14a.

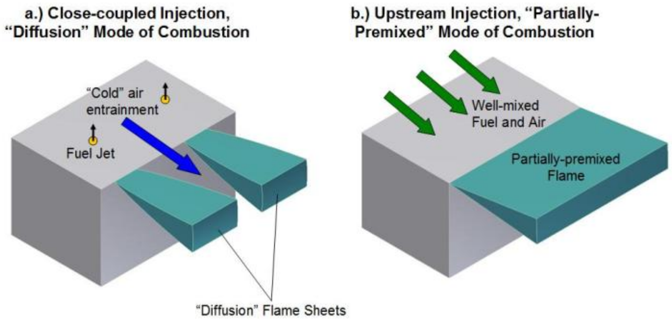

FIGURE 14: ILLUSTRATION OF HYPOTHESIZED SHEAR LAYER FLAME STRUCTURES FOR a.) CLOSE-COUPLED FUEL INJECTION b.) UPSTREAM FUEL INJECTION

The differences in flame "structure" illustrated in Figure 14 would explain the significant differences in near-wake shear layer CH* intensity that were observed between the two fuel injection configurations, as the line-of-sight integrated flame emission would be higher for the upstream fuel injection flame if it extended the entire span of the combustor. If the hypothesized flame structures illustrated in Figure 14 are correct, then close-coupled fuelling would allow passage of unburned, relatively cool gas between the flame sheets and into the recirculation zone behind the bluff body. This passage of air would cool the recirculated gases, resulting in smaller density gradients across the near-wake region of the flame when averaged across the span of the combustor. Thus, the suppressing mechanisms of dilatation and baroclinic torque upon the BVK instability are believed to have been much weaker for close-coupled fuelling than for upstream fuel injection due to the speculated differences in near-wake density gradients. The postulate that it is density gradients in the near-wake that ultimately control the onset and growth of the BVK instability has been addressed in previous studies [12, 18-19].

CONCLUSION

The dependence of the spatial distribution of the local equivalence ratio and the heat release dynamics upon the mode of fuel injection in liquid fuelled, bluff body-stabilized combustion was studied. A high-temperature, vitiated air stream was supplied to a single flame holder combustion channel which contained a 0.9 m long transparent section for optical access to the entire reaction zone. Liquid Jet-A fuel was injected into the inlet gas stream from one of two locations. In the first fuel injection configuration, the fuel was injected across the incoming gas stream from a cylindrical fuel bar located upstream of the bluff body (0.5 m from the flame holder trailing edge). In the second, the fuel was injected by four discrete, "close-coupled" fuel injectors integrated within the bluff body 2.5 cm upstream of its trailing edge.

The time-averaged spatial distribution of the combustion process heat release was characterized by CH* and C_2* chemiluminescence imaging of the flame, and ratios of the C_2* to CH* light emission were used to characterize the local equivalence ratio. Significant differences in the spatial heat release and equivalence ratio distributions were observed between the fuel injection configurations, even when the global operating conditions (e.g., overall fuel-air ratio, inlet velocity and temperature) were nearly identical. Upstream fuel injection typically resulted in stronger CH* intensities in the shear layers than close-coupled fuelling. For close-coupled fuelling, the peak CH* intensity typically occurred along the centerline of the wake several bluff body widths downstream.

For each operating condition, the average C_2*/CH* value in the flame was calculated. Interestingly, this value was found to increase linearly with increasing global equivalence ratio for tests in which the fuel was injected upstream of the bluff body. This linear curve fit was found to be independent of inlet velocity. This result suggests the possibility of calibrating local C_2*/CH* measurements to yield quantitative values for the local equivalence ratio in combustion of Jet-A (though further work is needed to validate this statement). In contrast, the spatial averages of C_2*/CH* for the close-coupled configuration were found to be nearly the same for all operating conditions, regardless of the global equivalence ratio. Furthermore, this constant value equaled the same average C_2*/CH* value obtained when the fuel was injected upstream of the flame holder at globally stoichiometric conditions, suggesting that combustion resulting from close-coupled fuelling took place, on average, in stoichiometric flamelets throughout the combustor.

The oscillatory heat release was also characterized for each operating condition by recording high-speed movies of the flame at 24 kHz. Post-processing of the movies using two-dimensional Fourier analysis determined the frequencies and amplitudes of heat release oscillations due to von Kármán vortex shedding. The amplitudes of such heat release fluctuations were found to be significantly higher for close-coupled fuelling than for fuel injection well-upstream of the flame holder for all global fuel-air ratios, demonstrating the strong influence of the spatial fuel and heat release distribution upon the dynamics. The von Kármán heat release oscillation amplitudes were then compared with the corresponding time-averaged CH* intensities occurring in the near-wake shear layers for each operating condition. It was shown that operating conditions resulting in high amplitude von Kármán heat release oscillations were correlated with low CH* intensities occurring in the near-wake shear layers, which was generally the case with close-coupled fuel injection. Conversely, when the near-wake CH* intensity was high, the von Kármán heat release oscillations were suppressed. It is postulated that upstream fuel injection resulted in increased span-wise fuel-air mixing prior to burning in the bluff body wake, resulting in a hotter recirculation zone which suppressed the von Kármán instability more than the close-coupled case due to increased gas expansion. For close-coupled injection, it is hypothesized that entrainment of unburned gases into the recirculation zone occurred, resulting in even less dilatation and thus, stronger vortex shedding.

ACKNOWLEDGMENTS

This work was funded through the Pratt & Whitney Center of Excellence partnership established with Georgia Tech. The authors would also like to thank Creare Inc. (Darin Knaus, contract monitor) and the U.S. Naval Air Warfare Center (Gearle Bailey, contract monitor) for allowing the use of the high-speed camera for this study.

REFERENCES

[1] Zukoski, E. E., and Marble, F. E., "The Role of Wake Transition in the Process of Flame Stabilization on Bluff Bodies," *Combustion Researches and Reviews*, 1955, pp. 167-180.

[2] Zukoski, E. E., and Marble, F. E., "Experiments Concerning the Mechanism of Flame Blowoff from Bluff Bodies," *Proceedings of the Gas Dynamics Symposium on Thermochemistry*, Northwestern University, Evanston IL, 1956, pp. 205-210.

[3] DeZubay, E. A., "Characteristics of Disk-Controlled Flames," *Aero Digest*, Vol. 61, No. 1, July 1950, pp. 54-56.

[4] King, C., "A Semi-empirical Correlation of Afterburner Combustion Efficiency and Lean Blow Out Fuel-air Ratio Data with Several Afterburner Inlet Variables," NACA Report RM E57F26.

[5] Longwell, J., Chenevey, J., Clark, W., and Frost, E., "Flame Stabilization by Baffles in a High Velocity Gas Stream," *Third Symposium on Combustion and Flame and Explosion Phenomena*, p. 40-44, 1949.

[6] Najm, H., Paul, P., Mueller, C., and Wyckoff, P., "On the Adequacy of Certain Experimental Observables as Measurements of Flame Burning Rate," *Combustion and Flame*, v. 113, pp.312-332, 1998.

[7] Morrell, R., Seitzman, J., Wilensky, M., Lee, J., Lubarsky, E., and Zinn, B., "Interpretation of Optical Flame Emissions for Sensors in Liquid-Fueled Combustion," 39th AIAA Aerospace Sciences Meeting and Exhibit, Reno, Nevada, January 2001, AIAA Paper 2001-0787.

[8] Lee, J.G. and Santavicca, D.A., "Experimental Diagnostics for the Study of Combustion Instabilities in Lean Premixed Combustors," *Journal of Propulsion and Power*, v. 19 (5) p.735-750.

[9] Clark, T. and Bittker, D., "A study of the Radiation from Laminar and Turbulent Open Propane-air Flames as a Function of Flame Area, Equivalence Ratio, and Fuel Flow Rate," NACA RM E54F29, 1954.

[10] Nori, V.N. and Seitzman, J.M., "CH* Chemiluminescence Modeling for Combustion Diagnostics," *Proceedings of the Combustion Institute*, 32, 2009, p.895-903

[11] Roby, R. J., Reaney, J .E., and Johnsson, E. L., "Detection of Temperature and Equivalence Ratio in Turbulent Premixed Flames Using Chemiluminescence," *Proceedings of the 1998 Int. Joint Power Generation Conference*, Vol. 1, 1998, 593-602.

[12] Cross, C., Fricker, A., Shcherbik, D., Lubarsky, E., Zinn, B.T. and Lovett, J., "Dynamics of Non-premixed Bluff Body-stabilized Flames in Heated Air Flow," *Proceedings of ASME Turbo Expo 2010: Power for Land, Sea and Air*, Glasgow, Scotland, U.K., ASME paper GT2010-23059.

[13] Turns, S. *An Introduction to Combustion*, McGraw-Hill, 2000.

[14] Lieuwen, T., Shanbhogue, S., Khosla, S. and Smith, C., "Dynamics of Bluff Body Flames near Blowoff," *45th AIAA Aerospace Sciences Meeting and Exhibit*, 2007, Reno, Nevada, AIAA Paper No. 2007-0169.

[15] Kiel, B., Garwick, K., Lynch, A., Gord, J. R. and Meyer, T., "Non-Reacting and Combusting Flow Investigation of Bluff Bodies in Cross Flow", *42nd AIAA/ASME/SAE/ASEE Joint Propulsion Conference and Exhibit*, Sacramento, California, AIAA Paper #2006-5234

[16] Hertzberg, J. R., Shepherd, I. G., and Talbot, L., "Vortex Shedding Behind Rod Stabilized Flames," *Combustion and Flame*, Vol. 86, 1991, pp. 1-11.

[17] Shanbhogue, S., Husain, S., and Lieuwen, T., "Lean blowoff of bluff body-stabilized flames: Scaling and dynamics," *Progress in Energy and Combustion Science*, 35, pp. 98-120, 2009.

[18] Mehta, P.G., and Soteriou, M.C., "Combustion Heat Release effects on the Dynamics of Bluff Body Stabilized Premixed Reacting Flows,' AIAA Paper # 2003-0835.

[19] Yu, M. and Monkewitz, P., "The Effect of Nonuniform Density on the Absolute Instability of Two-dimensional Inertial Jets and Wakes," Physics of Fluids, A, Vol. 2, Issue 7, 1990.